Polarization Stark spectroscopy for spatially resolved measurements of electric fields in the sheaths of ICRF antenna

A. Kostic,[1,2,3,a)] K. Crombé,[1,4] R. Dux,[2] M. Griener,[2] R. Ochoukov,[2] I. Shesterikov,[2] G. Suárez López,[2] M. Usoltceva,[1,2,5] R. Casagrande,[1,2] E.H. Martin,[6] and J.-M. Noterdaeme[1,2]

[1)] *Department of Applied Physics, Ghent University, 9000 Ghent, Belgium*

[2)] *Max-Planck-Institut für Plasmaphysik, 85748 Garching, Germany*

[3)] *Ludwig Maximillian University of Munich, 80539 Munich, Germany*

[4)] *Laboratory for Plasma Physics, Ecole Royale Militaire/Koninklijke Militaire School, 1000 Brussels, Belgium*

[5)] *Université de Lorraine, 54000 Nancy, France*

[6)] *Oak Ridge National Laboratory, Oak Ridge, Tennessee 37830, USA*

A multi-channel spectroscopic diagnostic based on the Stark effect on helium lines was developed and implemented in IShTAR (Ion Cyclotron Sheath Test ARrangement) to measure the spatial distribution of electric fields across the radio frequency sheaths of the Ion Cyclotron antenna. Direct measurements of the DC electric fields in the antenna sheaths are an important missing component in understanding the antenna-plasma edge interactions in magnetically confined fusion plasmas since they will be used to benchmark theoretical models against real antenna operation. Along with the high-resolution Czerny-Turner monochromator and a detector with an intensifier, the hardware relies on the 2 chained set of linear-to-linear fibre bundles that provide seven optical channels capable of resolving an 8.4 mm region in the vicinity of the antenna's box. The diagnostic is supported with local helium gas puff, enabling it to operate in non-helium plasmas. Spatially resolved electric field was measured for two discharge configurations, one with and one without the ICRF antenna. The results show a clear difference in the shape of the DC electric field's spatial profile for the two cases studied, with the elevated values when the ICRF antenna was operating. This demonstrates the ability of the diagnostic to measure even small relative changes in the intensity of the electric field.

I. INTRODUCTION

In this report we present a new experimental scheme and an approach to resolve local electric fields across the width of the radio frequency (RF) sheaths of Ion Cyclotron antennas in magnetically confined plasmas. Gaining experimental insight into the electric field distribution across the RF sheaths surrounding the plasma-facing components of antennas used for heating and current drive in tokamaks, is an important missing ingredient for controlling the interactions between the antenna and the plasma edge in these devices.

For a magnetically confined fusion devices such as tokamak, plasma heating and current drive with waves in the ion cyclotron range of frequencies (ICRF) proved to be of great importance and reliability. The dominant, energy carrying mode of the ICRF wave is the Fast Wave, which is evanescent at low plasma densities. Therefore to assure good efficiency of these systems, the waves are launched from an ICRF antenna placed close to the high-density plasma. Consequently, ICRF antennas must be protected against the hostile plasma environment inside a tokamak vessel, with a limiting frame and a Faraday screen. The sheaths formed around these protective structures, which are either made out of tungsten or coated with tungsten or boron, in turn interact with the RF fields, causing damaging side effects that decrease the antenna's performance. Examples of such side effects, observed in several tokamaks, include the occurrence of the hot-spots on the limiter frames of ICRF antennas and increased tungsten or boron impurity content in the main plasma due to sputtering of the limiters[1–3].

The underlying cause of the stated side effects to antenna operation is the rectified RF potential in the sheath surrounding the antenna's plasma-facing components, which arises from the interaction between the plasma, the components and electromagnetic waves[4,5]. Because of the rectified RF potential in the sheath, the ions are accelerated out of the plasma with velocities greater than the Bohm velocity, resulting in higher sputtering yields. To fully comprehend this phenomenon, it is important to experimentally quantify the DC electric fields that arise in the RF sheaths around the antenna's limiters, and are established parallel to the background magnetic field.

The main requirements for the measurements of electric fields in the ICRF antenna sheaths are for the diagnostic tool to be (i) contactless and non-invasive, not to disturb the boundary conditions of the physics to be studied, and (ii) to deliver the data with good spatial resolution. To address the requirement (i) the diagnostic we present here is based on polarization spectroscopy with electric fields assessed from the Stark effect on neutral helium emission lines. In particular, we are exploiting the Stark effect on the triplet 447.147 nm line originating from the 4^3D - 2^3P transition. The Stark effect on helium emission lines has been studied thoroughly[6–8] and applied in our earlier work[9]. The further advancement we report here is in terms of the equipment that enables spatial resolution (the diagnostic requirement (ii)), from

[a)] Author to whom correspondence should be addressed: ana.kostic@ipp.mpg.de

sheath-integrated[9] to sheath-resolved measurements.

II. STARK EFFECT ON 4^3D - 2^3P HELIUM TRANSITION - a brief overview for diagnostic purposes

Non-invasive measurements of the electric field in plasmas are based on spectroscopy. It is often a practice to use the Stark effect to evaluate the intensities of electric field directly from the recorded spectra. This was implemented in our work as well[9]. In this section we will briefly recall the underlying physics applied for the diagnostic purposes.

When exposed to an external electric field the atom becomes polarized. This causes an energy shift of its levels, hence the wavelength shift of the spectral line corresponding to the particular transition between them, known as the Stark effect. The energy shifts resolve the otherwise degenerated energy levels into the sub-levels, making the observable manifestation of the Stark effect directly linked to the magnetic quantum number of sublevel, denoted with m. This further implies that the effect manifests itself with different magnitude for the components of distinct polarization - the Stark shifts of the components polarized parallel to the external field (typically called π components, associated with the change in magnetic quantum number $\Delta m = 0$) are more pronounced than those of the components polarized perpendicular to the external field (σ components, with $\Delta m = \pm 1$).

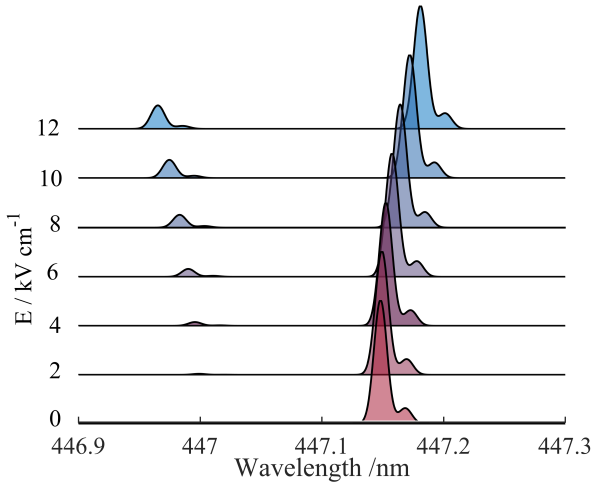

Figure 1. Wavelength shifts of 4^3D - 2^3P π components, calculated with the EZSSS for different electric field strength.

The theoretical treatment of the Stark effect is based on the method of perturbation theory in quantum mechanics, and as such it is independent of the plasma parameters. Figure 1 demonstrates the wavelength shifts of spectral lines of helium with increasing strength of the electric field denoted by E. The figure consists of several outputs of the Schrödinger equation solver: the EZSSS code (Explicit Zeeman Stark Spectra Simulator)[10]. The code first calculates the energy shifts for the levels involved in a selected transition due to the influence of the electric field. From these energy shifts EZSSS then derives the discrete spectral lines including now also the resolved non-degenerate levels. As the final output, shown in Fig. 1, EZSSS provides continuous spectra which are obtained by convoluting the discrete spectral lines with the broadening mechanisms such as an instrumental function of the set-up and the Doppler broadening, to make the theoretical output directly comparable to the experimentally obtained spectral profiles. The transition chosen for these calculations is the 4^3D - 2^3P of neutral helium. EZSSS was instructed to isolate the π components, and to position the background magnetic and electric field vectors parallel to each-other and perpendicular to the line of sight, as would be the case in the experiment.

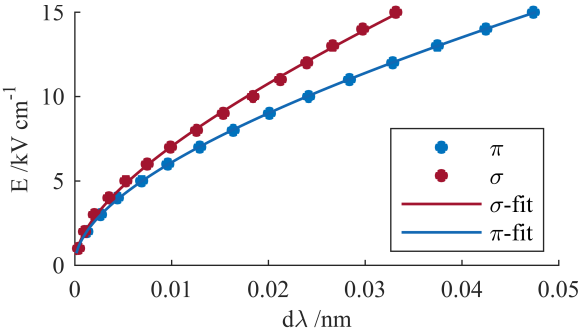

Figure 2. Comparison of the calculated wavelength shifts of π and σ components with increasing electric field strength.

Finally, the phenomenon of the Stark effect is put into practical use with polarization spectroscopy. This is achieved by evaluating the shift of the observed spectral line from its unperturbed wavelength, and connecting this shift to the electric field that has caused it. The applicable relation between the two is illustrated on the Fig. 2, with the Stark shifts denoted by $\mathrm{d}\lambda$ as an abscissa and the electric field strength as ordinate. The blue curve plotted here represents the same outputs of the EZSSS code as the ones shown in the previous figure, with $\mathrm{d}\lambda$ as the wavelength shift of the strongest component. The red curve is the EZSSS calculation for the isolated σ polarisation. To maximise the sensitivity of our scheme, we will focus only on the π polarization, and evaluate the electric field strength using the following relation (described with a blue solid line in Fig. 2):

$$\mathrm{E}(\mathrm{d}\lambda)\Big|_{\lambda_0} = 65.91 \times \mathrm{d}\lambda + 54.35 \times \mathrm{d}\lambda^{0.5}, \qquad (1)$$

with E in the units of kV cm^{-1}, and $\mathrm{d}\lambda$ in nm, evaluated for $\lambda_0 = 447.147$ nm.

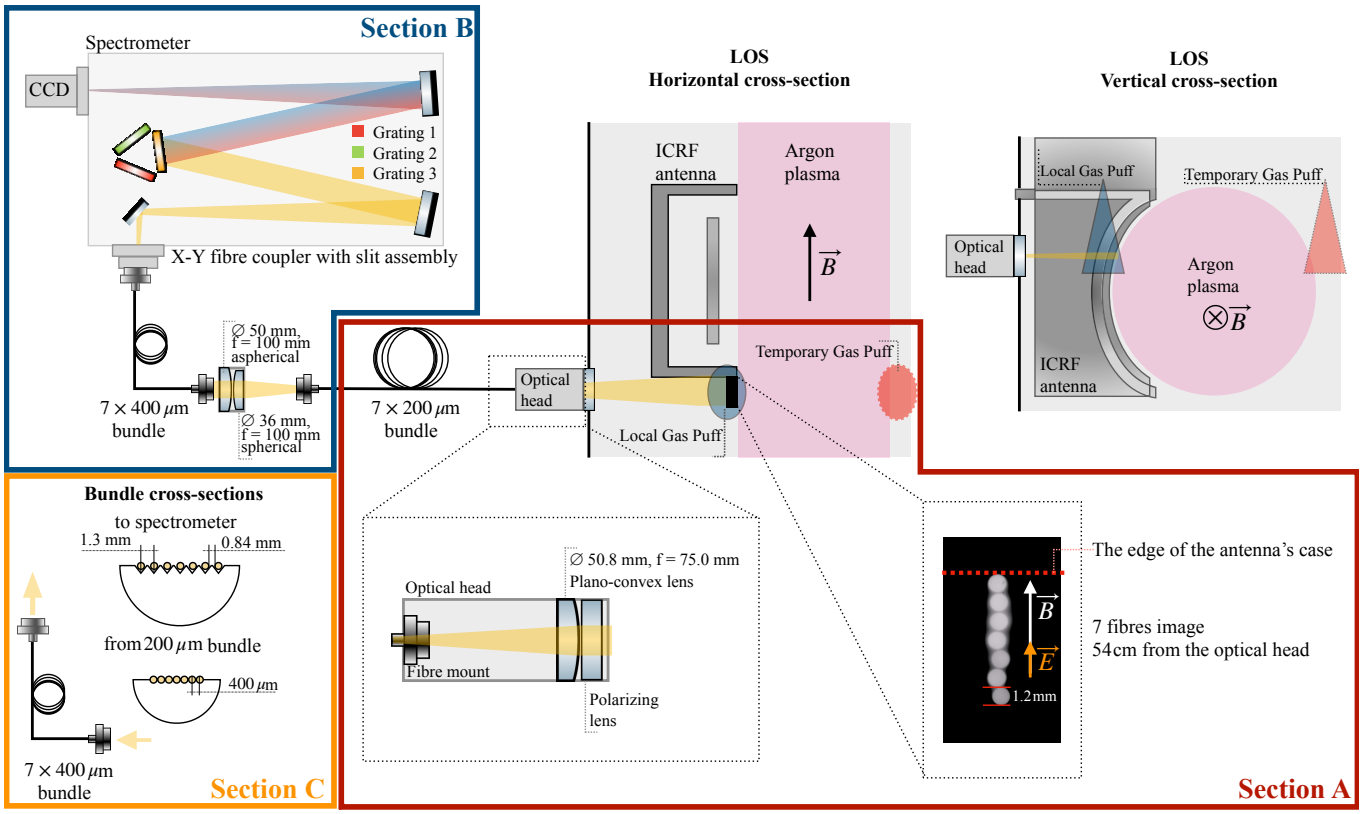

Figure 3. Schematics of spectroscopic system and implementation in the vicinity of IShTAR's ICRF antenna.

Line Selection

The experimental device used to develop and test the presented diagnostic can operate with either helium or argon plasma. Our choice of helium as a diagnostic medium was then made easier, since the Stark effect on helium lines has a well-developed and thoroughly-studied theoretical treatment, as mentioned in the introductory section.

The simple reason behind choosing the 4D-2P triplet, or the corresponding 447 nm spectral line, is that the signal-to-noise ratio was the highest for this particular line in the spectra recorded during the experiments. As the prime quantum number, n (= 4, 2), increases, so does the sensitivity of a transition to an external electric field, while the emission intensity decreases. Bound by the environment in which our experiments were conducted, this atomic transition was the optimal balance between the two.

III. EXPERIMENTAL SET UP

A dedicated linear device, IShTAR (Ion Cyclotron Sheath Test ARrangement), has been set up for experimental ICRF sheath physics studies. It provides easy access to the necessary diagnostics in a simplified geometry compared to a tokamak, while replicating the typical tokamak plasma edge environment in terms of the plasma density and the electron temperature[11].

IShTAR is equipped with a single strap ICRF antenna that was used to conduct the experimental verification of the diagnostic presented in this report. The ICRF antenna is installed in IShTAR's main vacuum chamber and designed to follow the shape of the plasma column. IShTAR's plasma is created in a helicon plasma source, thereby reaching electron densities of the order of $10^{17}\,\mathrm{m}^{-3}$ and electron temperatures close to 10 eV.

Two sets of magnetic field coils are looped around both the main vacuum chamber (a pair of larger coils in a Helmholtz-like configuration, later referred to as the "Big Coils") and the helicon plasma source (a set of 5 "Small Coils"), providing magnetic field along the main axis of the machine.

A. Spectroscopic equipment and integration

Figure 3 shows the schematic sketch of the spectroscopic equipment and its implementation in IShTAR, with the device's horizontal (axial) and vertical (radial) cross-section at the diagnostic location. Beside the device's cross-sections, the rest of the figure is divided in Section A: enclosing the "to the experiment" part of the diagnostic scheme, Section B: encircling what is called "the monochromator part" and Section C where the cross-

sections of the two ends of a custom-made bundle with 7 400 µm-fibres are sketched.

A glass port, located behind the ICRF antenna, provides a good location for the view-lines for the electric field measurements across the sheath of the antenna, parallel to the magnetic field lines. An optical head, with a focusing objective plano-convex Ø 2", f =75 mm lens, images the area of interest, 1.2 mm × 8.4 mm, onto the front face of the linear fibre bundle (1.55 mm line length). The optical head's custom-made design provides sufficient space to install additional optical components when necessary. An example is a linear polarizer mounted inside of the 60 mm cage rotation mount which allows for the selection of the polarization plane (σ or π). The fibre bundle contains 7 silica/fluorine-doped silica step-index fibres, arranged at both ends in a linear configuration (commercially available from Thorlabs, BFA200HS02). Each fibre within this bundle has a 0.22 numerical aperture and 200 µm core diameter. The location of the lines of sight, optical head design and the image projection from the 7 200 µm fibres focused at the location of measurements are singled out in Section A of Fig. 3.

We use an Andor Shamrock 750 spectrometer to resolve the fine Stark shifts of the 447.147 nm line in electric fields of up to 15 kV/cm. This spectrometer, in the Czerny-Turner optical design, has a focal length of 750 mm and an aperture of f/9.7. It is equipped with three 68 × 68 mm gratings of 600, 1200 and 3600 lines/mm. For our diagnostic purposes, to obtain the highest spectral resolution this arrangement can provide, we are using the grating with the highest number of lines per mm, labeled as the Grating 3 in Section B of the Fig. 3. The slit size is set to 15 µm, the optimal balance achieved between the signal intensity and the sharpness of the image (the Full Width at the Half of the Maximum of the spectral line). The instrumental function of the optical arrangement is 0.01 nm, or about 6 pixels.

Even though this optical arrangement of the Andor's 750 Shamrock spectrometer is providing very high spectral resolution, it introduces elongations of the signal in the vertical-pixel axis at the detector. Due to this elongation the individual images of the fibres within the bundle start to overlap on the detector's plane. To avoid the overlap of the optical signal, the additional optical setup was installed between the free-end of the 1.55 mm fibre bundle and the entrance slit of the spectrometer, as depicted in Section B of Fig. 3. These additional optical components first double the fibre image from 200 µm to 400 µm, with a 36 mm spherical and a 50 mm quartz aspherical lens, both with a focal length of 100 mm. The enlarged image is then projected on the secondary, custom-made fibre bundle that consist of 7 400 µm fibres also arranged in a linear-to-linear configuration but with an added spatial separation between the fibres on the end connected to the ferrule in front of the entrance slit of the spectrometer, as shown in Section C on the Fig. 3.

The optical signal is finally registered with the Andor's iStar 334 CCD detector with 1024 × 1024 px array

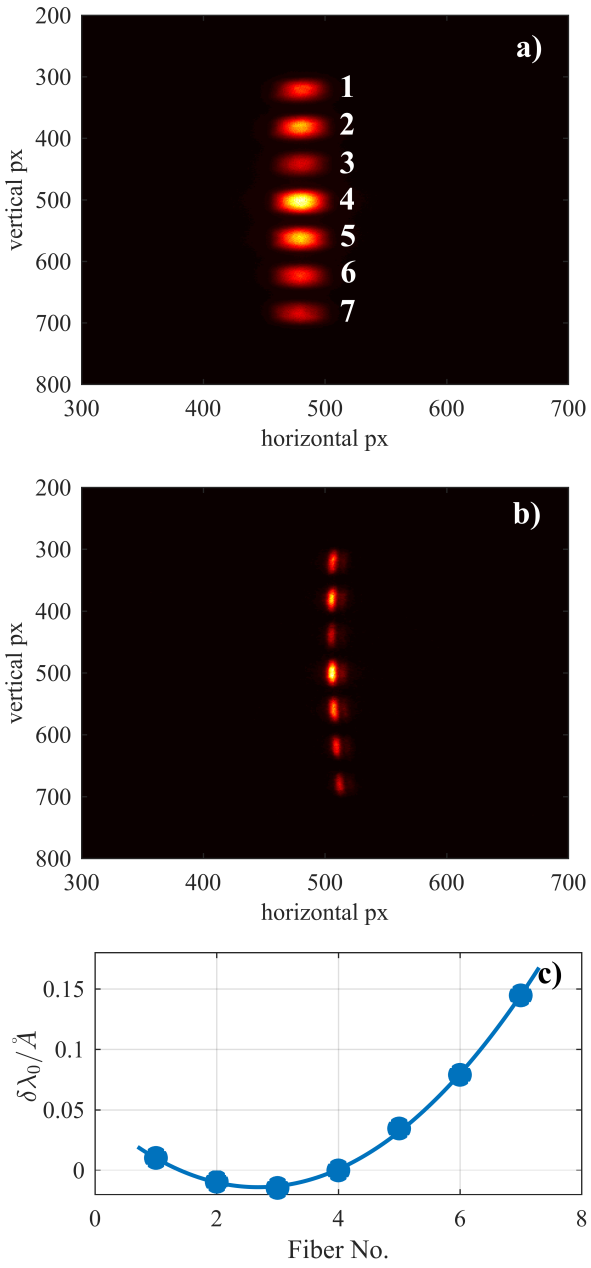

Figure 4. The image of the fibre bundle on the detector plane with the helium calibration lamp as the light source, (a) with the grating at the 0th order and the slit fully open, and (b) grating at the 1st order, fibre 4 cantered on the 447.147 nm line, slit width 15 µm. (c) Inherited parabolic displacement of the calibration signal on the detector. The equation describing the parabola is $f(x) = 0.0085 \times x^2 - 0.04557 \times x + 0.04716$.

installed at the spectrometer's output port. The image that the detector sees when the grating is in the 0th order is shown in Fig. 4 (a), with the slit being completely open. Because the optical signals from individual fibres do not overlap, they can be binned within the corresponding vertical pixels of each fibre. When the grating is centred on the 447.147 nm in the first order, the op-

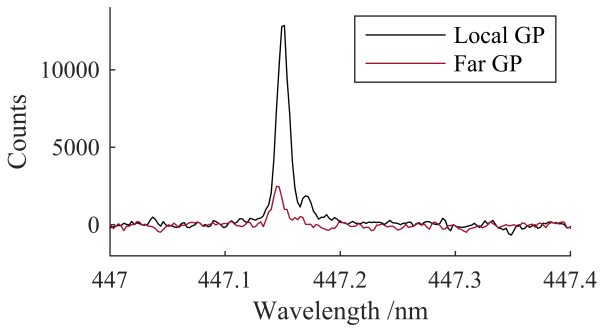

Figure 5. Comparing the raw spectra recorded when the gas puff was local (black) and when it was on the opposite side of the plasma column with respect to the location of interest (red).

tical signal that the CCD detector of the spectrometer sees, with the slit width set to 15 µm, is shown in Fig. 4 (b). The light source used for the two images on this figure is a helium calibration lamp. It is important to stress here the typical parabolic shape with respect to the wavelength axis of the optical signal when the grating is in the first order, as it must be taken into account when evaluating the shifts due to electric field.

The parabolic shape with respect to the wavelength axis of the calibration lamp image is isolated in Fig. 4 (c), where each point represents binned signal corresponding to a track associated with a certain fibre and its relative shift from the centred 447.147 nm, i.e fibre number 4. The shifts here are in the units of Å, and marked as $\delta\lambda_0$ to differentiate them from the Stark shifts.

Local helium gas puff

For the purposes of this diagnostic, a localized helium gas puff is installed to decouple the optical signal originating in the sheath region near the ICRF antenna box from the bulk plasma contribution and ensure local measurements, while the main IShTAR plasma is created with argon.

After testing different percentages of the two gasses, the lowest helium gas flow rate (to avoid disturbing local plasma density and overall plasma performance) providing a decent optical signal for the 447.147 nm line, is set to 60 sccm, or 2.7×10^{19} helium atoms per second, with 10 sccm argon at base pressure $p = 2.5 \times 10^{-3}$ mbar. Helium is delivered through a gas tube installed above the area of interest.

Unlike in a tokamak environment where the neutral gas becomes ionized once it passes into the bulk plasma, neutral helium atoms in IShTAR remain in the device's main vacuum chamber, moving freely since they are not influenced by the magnetic field. Therefore, in order to validate that the strongest optical signal will actually originate from the region of interest, a gas tube was put

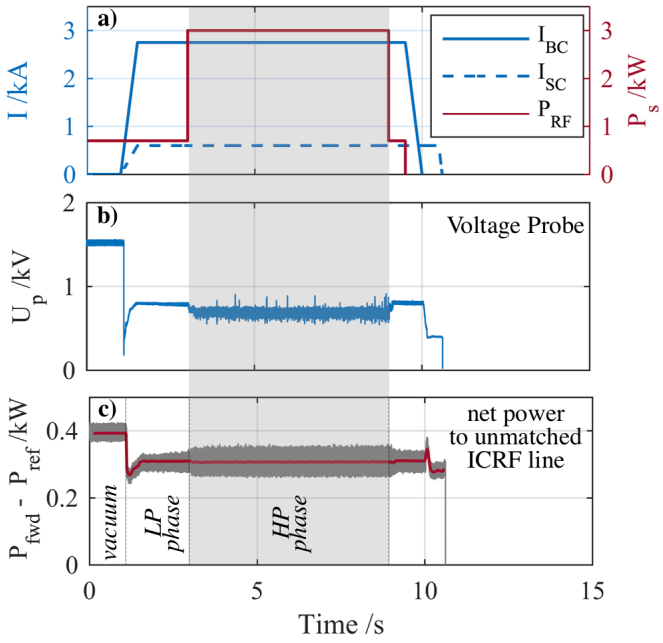

Figure 6. Time traces of the operational parameters. (a) I_{SC} and I_{BC} are referring to the current in the Small and the Big coils respectively. P_{RF} stands for the power delivered to the helicon antenna of the plasma source. The grey-shaded area marks the stable-plasma phase, with the overlapping flattops of the operational parameters, from $3 - 9$ s of the discharge. (b) Voltage probe data characterising the *ICRF ON* discharge. (c) Net power to the unmatched transmission ICRF line. The reduced net power as delivered from the generator is likely due to the altered matching conditions in the presence of plasma in front of the antenna.

temporarily on the side opposing the antenna, with the primary argon plasma in between, as sketched in Fig. 3. For the same acquisition parameters and the plasma environment, the two spectra recorded with the regular location of the gas puff (Local GP, black curve) and the displaced tube (Far GP, red curve) are compared in Fig. 5. Here it can be seen that even the contribution of a continuously puffed helium cloud behind the plasma, which could be the worst-case scenario, does not significantly affect the local measurements.

Even so, the Stark shifts on the spectral lines of helium could only occur in the presence of a strong background electric field, which is, along the entire stretch of the lines of sight, found only in the region of interest.

IV. DATA TREATMENT AND DEMONSTRATIVE RESULTS

To demonstrate the diagnostic, it was used to resolve the electrical fields across the sheath that forms around the ICRF antenna box in IShTAR. From the discharges that used this diagnostic we will be showcasing the two for which the time-traces of the operational parameters

are shown in Fig. 6 (a). The only distinction between the compared discharges, as long as the operational parameters are concerned, was that the power was supplied to the ICRF antenna in one, but not in the other (referred to as *ICRF ON* and *ICRF OFF* discharges respectively). The left ordinate axis in the Fig. 6 (a) represents the current through to the two sets of coils, while the right ordinate axis corresponds to the RF power levels delivered to the helicon antenna. The grey-shaded area marks the stable-plasma phase. During the stable phase, the magnetic field created along the main axis of the machine was 93 mT at the area of interest, which is too low for the Zeeman effect (the magnetic-field analogue of the Stark effect) to be noticed on the recoded optical emission spectra.

When used, the ICRF antenna operated at 5.9 MHz and was matched in vacuum by a variable capacitor and inductor, which are tuned prior to a plasma discharge. The unmatched side of the transmission line is diagnosed by a voltage probe at about $\sim$ 5 m from the antenna feedthrough and the coupled power to it by a directional coupler behind the matching components. These measurements combined provide a qualitative estimate of the voltage standing wave ratio in the line, and the time traces can be seen in Fig. 6(b) and (c). Three phases are clearly distinguishable: vacuum operation with 0.4 kW of coupled power and a voltage of 1.5 kV and plasma operation with 0.31 kW of coupled power in: low-power helicon at a voltage of 800 V and high-power helicon at 700 V. Two features are apparent from the measurements: a clear reduction of the voltage absolute value at the probe location when going from vacuum to helicon plasma operation (although the coupled power is also reduced), and the manifestation of turbulent structures when the ICRF antenna is operated in high-power helicon mode. Future upgrades of the ICRF transmission line diagnostics may allow for the complete measurement of the antenna loading impedance, but these are not implemented at the moment.

During the experiments, the spectra were recorded in a kinetic series of 11×1 s of exposure time. The readout mode was set for a Multi-Track defined in such a manner that each track bins the vertical pixels associated with one fibre. Although the kinetic series cover the entire discharge duration, we focused on the spectra recorded during the stable-plasma phase for the results shown.

In post-processing, the data from the experiments and the calibration lamp is first cleaned by subtracting the corresponding dark spectra. All recorded signals are then normalised to unit area to allow a visual comparison of the spectra. Normalised spectra from the calibration lamp, the discharge without and the discharge with an ICRF power are presented in Fig. 7. The dots are representing recorded data, while the lines are the fitting routine's final output. The figure shows only 6 out of 7 fibres since the signal on the seventh fibre for the discharges with an ICRF antenna being ON is too noisy to fit the peak properly. Since we use the Stark shift of the

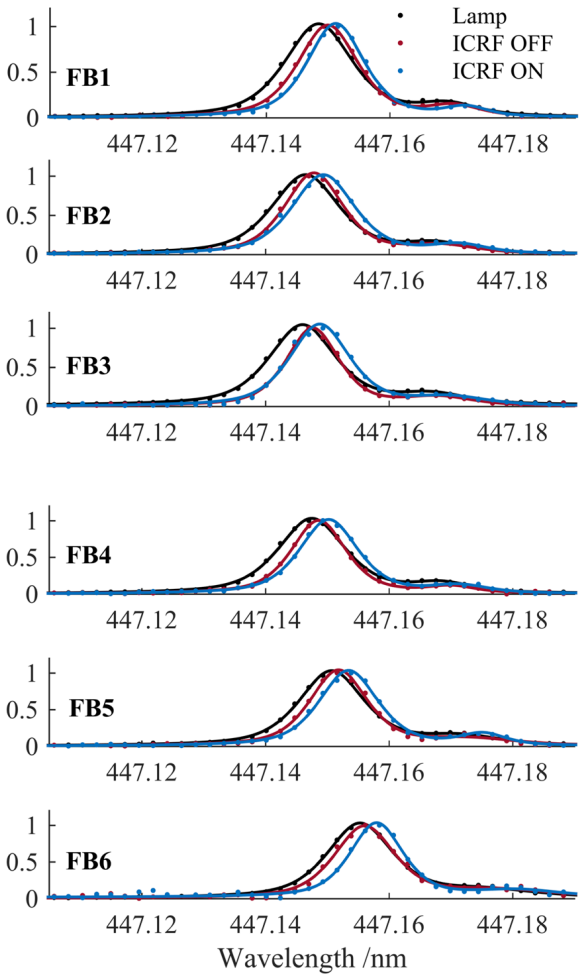

Figure 7. Normalized spectra from the helium calibration lamp (black), a discharge without (red) and a discharge with an ICRF antenna (blue) for the 6 fibres in a bundle from the one closest to the ICRF antenna box (FB1) to the one 8.4 mm away from it.

line from its unperturbed wavelength to determine the strength of the electric field that caused it, in our case the unperturbed line will be the one from the calibration lamp of helium. In Fig. 7, the Stark shifts are already visible, being more pronounced on the spectra recorded when the ICRF antenna was used during the discharges. Fibres ordered from the one closest to the ICRF antenna box (**FB1**) to the one farthest, 6.6 mm, away (**FB6**) are labeled as **FB1-6** in the Fig. 7.

The central wavelength of the main peak in each spectrum is extracted from a pseudo-Voigt fit on the spectral line. The fitting routine is performed for $N = 100$ trial runs and the best fit is saved, i.e the one with the lowest fitting error. Since this fit is solely mathematical, a statistical weighting has been performed to maximise the precision, and the same procedure has been repeated to compare 50 best fits for each line fit. The most frequently occurring central wavelength is then chosen for the Stark

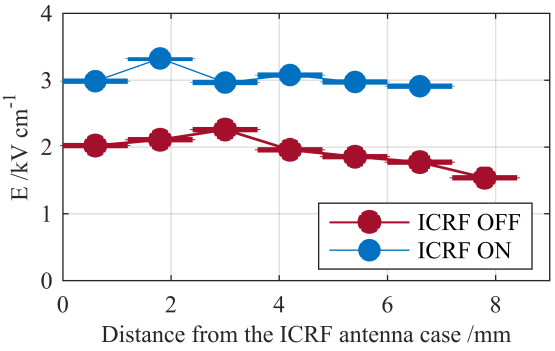

Figure 8. Electric field measured evaluated across the sheath of the antenna's box for the discharge without and with the ICRF antenna.

shift estimates, with an accuracy of the fit of 10^{-6} nm.

The measured Stark shifts are then introduced in Eq. 1. The electric fields evaluated as the final result of this diagnostic equipment are presented in Fig 8. The fields are resolved across the sheath and the horizontal axis, being the distance from the ICRF antenna case, is calibrated with respect to the centre of the image of each fibre at the location of measurements with the horizontal error bars corresponding to their diameter.

The results for the discharge with the ICRF antenna being OFF are in red. Here we see the anticipated decrease of the electric field over the 8.4 mm broad region from the antenna's case. We must note that our initial estimates of the area to be scanned were based on the Langmuir probe measurements of radial electron density for different discharge configurations, which were of the order of $10^{15} - 10^{17}$ m^{-3}. However, the location of the electric field measurements is in the shadow created by the ICRF antenna casing, but also in the close proximity of a machine's metallic back flange, where the electron densities are greatly reduced. Consequently, the red curve in Fig. 8 would eventually have fallen to 0 kV cm^{-1}, and this does not occur in the region covered by the lines of sight as the sheath is much wider than expected. In addition, when analyzing this figure, it should be taken into consideration that even in the *ICRF OFF* scenario, the RF fields are still present in IShTAR's plasma due to the helicon source which is magnetically connected to the metallic surfaces in the main chamber where the measurements were carried out. This further complicates the simplistic (steady-state-like) calculation of sheath thickness and the estimate of electrical fields within it.

The results in blue are the electric fields across the sheath for the discharge which used the ICRF antenna. As anticipated, these fields are higher than in the previous scenario. The flattened behaviour of the evaluated data, but also the undeniable influence of the surrounding plasma environment on the electric field in the sheath is to be the subject of a study with the additional diagnostic tools in place, such as Langmuir probes close to the area of interest, aided with the appropriate theoretical models of RF sheath. In this paper we limit ourselves on the demonstration of the capabilities of the diagnostic.

V. CONCLUSIONS

To summarise, we have developed an easy-to-use and easy-to-implement diagnostic scheme based on the polarization Stark spectroscopy to spatially resolve the electric field across the sheath of an ICRF antenna in magnetically confined plasmas. The diagnostic equipment described in this article comprizes of a high resolution spectrometer in the Czerny-Turner optical arrangement and a pair of fibre-bundles resolving 8.4 mm in 7 points. The measurements are aided with a local gas puff.

The theoretical background of the method is a well-described Stark effect on helium atom. For a given geometry (respective orientation of the magnetic and electric field vectors, and the line of sight), selected polarization plane and the electric field strength a Schrödinger equation solver - the EZSSS code was used to provide a relation between the Stark shift of the chosen 447.147 nm spectral line and the electric field that influenced it. Since the calculations are based on the perturbation theory, the method is independent of plasma parameters such as plasma density or temperature.

The diagnostic capabilities in non-helium plasmas are demonstrated by results obtained for plasma discharges whose operation parameters differ only in whether or not ICRF was used. As such, the presented diagnostic has a promising ability to assist the experimental research of the RF sheaths introduced by the ICRF antennas.

ACKNOWLEDGMENTS

The authors are grateful to the following for their help with the regular IShTAR operations and this project: F. Fischer, H. Faugel, H. Fünfgelder and G. Siegl.

This work has been carried out within the framework of the EUROfusion Consortium and has received funding from the Euratom research and training programme 2014-2018 and 2019-2020 under grant agreement No 633053. The views and opinions expressed herein do not necessarily reflect those of the European Commission.

The work was also supported by the Research Foundation - Flanders (FWO), with project number G0B3115N.

REFERENCES

[1] M. Bures, J. Jacquinot, K. Lawson, M. Stamp, H. P. Summers, D. A. D'Ippolito, and J. R. Myra, Plasma Physics and Controlled Fusion **33**, 937 (1991).

[2] S. J. Wukitch, B. Lipschultz, E. Marmar, Y. Lin, A. Parisot, M. Reinke, J. Rice, and J. Terry, Journal of Nuclear Materials **363-365**, 491 (2007).

[3]V. Bobkov *et al.*, Plasma Physics and Controlled Fusion **59**, 014022 (2017).
[4]J. Myra, D. D'Ippolito, and M. Gerver, Nuclear Fusion **30**, 845 (1990).
[5]J.-M. Noterdaeme and G. Van Oost, Plasma Physics and Controlled Fusion **35**, 1481 (1993).
[6]C. C. Klepper *et al.*, Physical Review Letters **110**, 215005 (2013).
[7]E. H. Martin *et al.*, Plasma Physics and Controlled Fusion **57**, 065011 (2015).
[8]N. Cvetanović, M. M. Martinović, B. M. Obradović, and M. M. Kuraica, Journal of Physics D: Applied Physics **48**, 205201 (2015).
[9]A. Kostic, R. Dux, K. Crombé, A. Nikiforov, R. Ochoukov, I. Shesterikov, E. H. Martin, and J.-M. Noterdaeme, Review of Scientific Instruments **89**, 10D115 (2018).
[10]E. H. Martin, *Electric field measurements of the capacitively coupled magnetized RF sheath utilizing passive optical emission spectroscopy*, Doctor of philosophy, North Carolina State University, Raleigh (2014).
[11]K. Crombé *et al.*, in *Plasma science and technology : basic fundamentals and modern applications* (IntechOpen, 2019).